ACS Catalysis

pubs.acs.org/acscatalysis

Research Article

# Influence of Fuels and pH on the Dissolution Stability of Bifunctional PtRu/C Alloy Electrocatalysts

Attila Kormányos,* Florian D. Speck, Karl J. J. Mayrhofer, and Serhiy Cherevko*

Cite This: *ACS Catal.* 2020, 10, 10858–10870

Read Online

ACCESS | Metrics & More | Article Recommendations | Supporting Information

**ABSTRACT:** The application of organic fuels in fuel cells is an attractive way to circumvent the major drawbacks of hydrogen as an energy carrier, yet catalysis is still a bottleneck for efficient oxidation. One of the most promising bifunctional anode catalysts is PtRu, which has proven to be the state-of-the-art electrocatalyst in alcohol oxidation processes. While plenty of works so far have addressed the activity and mechanism of oxidation reactions on PtRu, less is known about the influence of organic fuels on the stability during operation. In this contribution, the effect of isopropanol, methanol, ethanol, formic acid, ammonia, and carbon monoxide on the stability of carbon-supported PtRu was studied both in acidic and alkaline media. The scanning flow cell coupled to an inductively coupled plasma mass spectrometer (online ICP-MS) technique allowed the tracking of dissolution events that occurred during the applied electrochemical protocol in real-time. Our main conclusion is that PtRu/C remained stable in the operation range of fuel cells. In addition, if the upper potential limit was further increased PtRu/C was less stable in alkaline medium in which, if compared to acidic electrolyte, approximately 4-times higher Ru and 14-times higher Pt dissolution was measured in the absence of the studied fuels. The onset potential of dissolution was not affected by the presence of fuels (except CO), while dissolution rates were notably affected, most visibly in the case of isopropanol and ammonia in alkaline media and carbon monoxide in both acidic and alkaline media. The observed phenomena are briefly discussed underlining the necessity of more detailed and mechanistic studies to fully understand the reason behind dissolution processes in the presence of the investigated fuels.

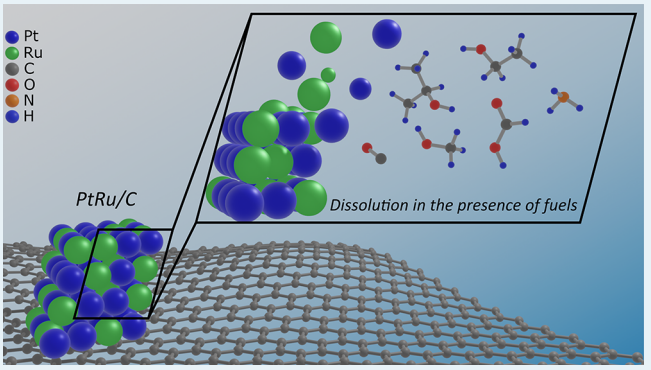


**KEYWORDS:** *fuel cells, stability, alloy electrocatalyst, platinum, ruthenium*



## 1. INTRODUCTION

Hydrogen is considered to be a promising candidate to play a key role as an energy carrier in the future's sustainable energy economy. However, it has certain disadvantages, which have to be addressed prior to its widespread application. One such disadvantage is its low volumetric energy density (e.g., 5.6 MJ $dm^{-3}$ in the case of hydrogen compressed to 700 bar) that is far less than, e.g. gasoline's (32 MJ $dm^{-3}$).[1] In addition, a complex infrastructure is needed for its safe (explosion hazard) storage and transportation, which is still not readily available.[2] One option to overcome these issues is to use organic fuels, such as alcohols (almost exclusively primary),[3] formic acid,[4] ammonia,[5,6] etc. Two decades ago significant efforts were made to develop fuel cells utilizing these chemical energy carriers, which are capable of competing with the proton exchange membrane (PEM) fuel cells. Despite the advanced research interest, no widespread breakthrough has been achieved so far. The major limitation of these systems is the sluggish oxidation kinetics due to the complex reaction mechanisms leading to low electrocatalytic activity.[6] Another significant problem is the poisoning of the anode electrocatalyst by strongly adsorbed intermediate species, such as CO formed during the oxidation process.[7−9]

Ammonia is a rather interesting fuel, among the ones mentioned above, since $N_2$ forms upon its oxidation making it a viable option to fabricate zero-emission fuel cells. The achievable current densities of such devices were rather low (1−10 mW $cm^{-2}$) until lately, when Gottesfeld et al. reported a record power density of 450 mW $cm^{-2}$ at 100 °C operating temperature (with a platinum group metal (PGM) anode and a non-PGM cathode), which is a significant step for the application of direct ammonia fuel cells in the transportation sector.[5]

An alternative approach to tackle the shortcomings of $H_2$ is to use liquid organic hydrogen carriers (LOHC). LOHC

Received: May 11, 2020
Revised: August 28, 2020
Published: August 31, 2020




https://dx.doi.org/10.1021/acscatal.0c02094
*ACS Catal.* 2020, 10, 10858−10870

systems typically consist of a liquid, "hydrogen-lean" aromatic compound, and its hydrogenated ("hydrogen-rich") counterpart.[10] This concept is particularly attractive because $H_2$ can be handled in high volumetric energy storage density under ambient conditions along with the usage of currently available infrastructure for transporting and distributing today's fossil fuels. The main disadvantage of the technology is that the dehydrogenation process, which is necessary to harvest $H_2$ from the LOHC, is endothermal and requires a substantial input of energy.[11] A rather interesting option to solve this problem was proposed recently:[10] transfer hydrogenation from H18-DBT to acetone and the direct use of the formed 2-propanol as a fuel in a PEM fuel cell.

Fuel cell technology can be industrially relevant only if high power densities are achieved with the ability to maintain the achieved performance as long as possible (e.g., the lifespan of the operated vehicle) at a reasonable cost. Electrocatalysts used both on the anode and cathode side are the cornerstones to fulfilling all these requirements. Most research efforts in electrocatalysis focus on improving activity, thus the amount of catalyst (this is especially important for noble metals) can be decreased, resulting in lower manufacturing costs.[12] However, the stability of the catalyst becomes extremely important when such low amounts are used, because even minor losses can significantly deteriorate device performance.[13,14] The decrease of fuel cell performance is mostly attributed to the degradation of the cathode electrocatalysts, however, the stability of the electrocatalysts employed on the anode side is equally important. For example, the performance of a direct methanol fuel cell using PtRu/C as an anode electrocatalyst can be dropped by as much as 20−30% just during a long-term durability test.[15−17] This effect was attributed to the degradation of PtRu[13,14] and the crossover and subsequent deposition of Ru on the cathode.[15,17,18] As it is visible, selective dissolution of one component can be a significant issue in bimetallic catalysts.[19] Hence, this example underlines that it is vital to understand degradation processes that could occur during the operation of the fuel cell. Dissolution, as it has been mentioned above, is one of the most important among those mechanisms and has been extensively studied in the past few years for single metals such as Pt,[12,20] Ir,[21] Ru,[21] Rh,[22] etc. both in acidic and alkaline media. On the other hand, the stability of catalysts can be greatly influenced by many factors, such as ions and other species present in the solution,[12,23] pH,[24] support,[25] alloying,[14] etc. Valid predictions on long-term performance, however, demand actual measurements under these conditions. A versatile tool to track dissolution in parallel with running an electrochemical protocol is to couple an electrochemical cell to an ICP-MS (online ICP-MS). This unique technique, developed in our lab, allows the time-resolved quantification of even trace amounts of elements during electrochemical measurements giving invaluable insights on dissolution/degradation mechanisms. More information on the method and its featured applications can be found in our previous reports.[26−28]

Oxidation of fuels on the surface of the electrocatalyst is usually a very complex process,[29−31] involving a set of elementary reaction steps such as (i) adsorption of the reactant, (ii) intermediate formation, (iii) product formation, and (iv) desorption of the formed product from the catalyst surface. Activity relies greatly on how strongly the intermediates are adsorbed on the metal surface, however, it is still not clear how they affect the stability of the given electrocatalyst. It has been already demonstrated that CO, which is a common intermediate formed during the oxidation of primary alcohols, drastically decreases the stability of Pt by a factor of almost four.[23,32] The reason behind this phenomenon is that the adsorbed CO enhances Pt dissolution during the cathodic scan by blocking reduced Pt sites and, hence, preventing redeposition of the dissolved metal ions. In addition to this effect, the complexation of Pt can also happen in parallel with the formation of Pt-carbonyls. Fewer reports can be found for the effect of various other fuels present in the electrolyte solution on the stability of the electrocatalyst. To address this issue, PtRu was chosen as a model catalyst system, since it is the state-of-the-art bifunctional electrocatalyst applied for the electrocatalytic oxidation of primary alcohols such as methanol[33] and ethanol.[33,34] To our knowledge, only the effect of methanol on its stability was addressed, and an increased Pt and Ru dissolution was experienced in its presence. It was assumed that the enhanced Ru dissolution is due to the consumption of surface oxides ($Ru_2O_3$), while increased Pt dissolution is due to inhibited redeposition and higher destabilization of the surface due to increased Ru dissolution.[35] Apart from this report, only ex-situ studies can be found on this matter, which were performed almost exclusively in the presence of primary alcohols[13,14,36]

In this study, the effect of various fuels on the stability of carbon-supported PtRu 1:1 electrode (simplified to "PtRu" in the text) is presented. The stability of PtRu was first investigated in the presence of primary and secondary alcohols. Further measurements were carried out in HCOOH- and $NH_3$-containing electrolytes. Although PtRu is not the most active alloy to oxidize these fuels, they are still included in our current work to map the stability of the alloy, as either Pt or Ru itself or their combinations with other elements might be proven to be useful in catalyzing $NH_3$- or HCOOH-oxidation, respectively. Finally, despite the fact that CO is not a fuel, it has been also selected, since it is the most common intermediate in primary alcohol- and formic acid-oxidation reactions and this is why it is essential to explore how it affects the degree and kinetics of dissolution. Stability data presented in this paper were collected both in acidic and alkaline electrolytes, and the effect of pH combined with the effect of different fuels on the stability of PtRu are discussed in detail. Hence, the main goal of this work is to benchmark and compare the dissolution stability of PtRu in the presence of different organic fuels, keeping other experimental parameters identical.

## 2. EXPERIMENTAL SECTION

**2.1. Chemicals.** $HClO_4$ (70%, Suprapur), KOH (Suprapur, ≥ 99.995%, VWR), isopropanol (ACS, 99.5+%, VWR), methanol (ACS, 99.8%, VWR), ethanol (ACS, EMSURE, 99.9%, VWR), formic acid (ACS, VWR) and $NH_4SO_4$ (99%, Merck) were all purchased from Merck and used without further purification. Carbon-supported PtRu (Pt:Ru 1:1) was purchased from Tanaka. Ar (99.999%), $H_2$ (99.999%) and CO (99.999%) were purchased from Air Liquide Deutschland GmbH. All solutions were prepared using ultrapure water (18.2 MΩ cm, TOC < 5 ppb) prepared by a Merck Millipore Milli-Q system.

**2.2. Preparation of Thin Films.** Thin films of PtRu were prepared on a glassy carbon (GC) substrate (SIGRADUR G, HTW 5 × 5 $cm^2$) by drop-casting. Prior to this step, all GC substrates were ground with SiC grinding paper (mounted on a


https://dx.doi.org/10.1021/acscatal.0c02094
ACS Catal. 2020, 10, 10858−10870

MD-Gekko disc) applying 300 N force, and 200 rpm rotation speed. The sample holder was counter-rotated during this procedure with 150 rpm. This was repeated at least two times using four different grain sizes: 220, 1000, 2000, and 4000 (corresponding to 68, 18, 10, and 5 $\mu$m grain size, respectively). Afterward, the GC electrode was polished with the same device on a MD-Mol (cat. Number: 40500079) polishing pad using DiaPro MD-Mol paste (water-based diamond suspension; particle size of 3 $\mu$m, Struers) with the following parameters: 150 N, 200 rpm, the sample holder was also counter-rotated with 150 rpm for 5 min. Flat GCs were cleaned with Kimwipes and isopropanol. Finally, the electrodes were rinsed with Milli-Q water, dried, and stored under ambient conditions overnight prior to drop-casting of the catalyst inks. For the ink preparation, 3.3 mg catalyst was dispersed in 1 mL ultrapure water and sonicated for 40 min with 25% intensity using a sonicating horn (Branson SFX 150). Sonication was on for 4 s, which was interrupted by a 2 s break. The dispersion was placed in an ice bath during sonication. Immediately after sonication 0.2 $\mu$L aliquots were pipetted and drop-cast on the GC substrate reaching approximately 20 $\mu$g cm$^{-2}$ metal loading. The spots dried under air at room temperature. The diameter and quality of each spot was determined using a laser scanning microscope (Keyence VK-X250) and ranged between 800 and 1000 $\mu$m. All electrochemical and dissolution data were normalized against the individual geometric surface area.

**2.3. Stability Measurements Using Online Inductively Coupled Plasma Mass Spectrometry.** Stability measurements were performed with a custom-built scanning flow cell (SFC) coupled to an inductively coupled plasma mass spectrometer (Nexion 300X, PerkinElmer). A graphite rod (99.995% trace metals basis, Sigma-Aldrich) was employed as a counter electrode, which was connected to the SFC on the electrolyte inlet. An Ag/AgCl/3 M KCl reference electrode (Metrohm) was connected to the SFC through a capillary channel in close proximity to the working electrode surface. The drop-casted spots on the GC substrate served as working electrodes. More detailed information on the setup can be found elsewhere.[26−28] All electrochemical protocols were carried out using a potentiostat (Gamry, Reference 600) during stability measurements. The GC plate with working electrodes was contacted with and XYZ translation stage (Physik Instrumente M-403), which also allowed the rapid screening of multiple electrocatalyst spots. All instruments (stage, peristaltic pump, gas control box, and potentiostat) were simultaneously controlled by a custom-made LabView software. The ICP−MS was calibrated daily by a four-point calibration slope made from standard solutions (Merck Centripur Pt, Ru, Re, Rh) containing the investigated metal ions in a given concentration in either 0.1 M $HClO_4$ or 0.05 M KOH solution. $^{187}$Re and $^{103}$Rh were used as internal standards. The purged electrolyte flow rate was controlled by the peristaltic pump of the ICP−MS (M2 pump, Elemental Scientific) and calibrated daily. The average flow rate was 3.54 ± 0.05 $\mu$L s$^{-1}$.

**2.4. Conditions and Protocols during the Electrochemical Measurements.** Electrochemical measurements were carried out either in acidic (0.1 M $HClO_4$) or in basic (0.05 M KOH) solutions. Five different fuels were tested in each medium. The concentration of all fuels (except CO where the electrolyte was saturated prior to measurements) were maintained at 0.05 M because of the limitations of the online ICP−MS due to the organic load. The list of all fuels along with the conditions are presented in Table S1 of the Supporting Information (SI). HCOOH was only measured in the acidic electrolyte because of precedent literature data, in which it was found that the performance of the electrooxidation of HCOOH is maximal at a pH close to its p$K_a$ value and rapidly decreases with increasing pH.[31] Additionally, electrooxidation of $NH_3$ was only investigated in basic electrolyte. The reference electrode was calibrated against a reversible hydrogen electrode (RHE) prior to the measurements as follows: the pH of the electrolyte solutions was measured at the beginning of each measurement day and used to convert the potentials measured versus the Ag/AgCl reference electrode to the reversible hydrogen electrode scale, using the following equation:

$$E_{RHE} = E_{applied} + E_{Ag/AgCl} + 0.0591 \times pH,$$
$$\text{where } E_{Ag/AgCl} = 0.197V$$

In the case of the acidic electrolytes, the pH was identical to the pH of pure 0.1 M $HClO_4$ − pH ≈ 1. While in the case of the alkaline measurements, the pH was identical to the pH of pure 0.05 M KOH − pH ≈ 12.5. The only exception was if $NH_3$ was present in the electrolyte in which case the pH decreased to ∼9.2. Two electrochemical protocols were used as follows: catalyst spots were contacted by the SFC close to the open circuit potential (+0.05 $V_{RHE}$) and a potentiodynamic measurement was started shortly after. The first protocol consisted of five cyclic voltammograms (CV) starting at 0.05 $V_{RHE}$ and going to five different upper potential limits (UPL, +0.3, +0.6, +0.9, +1.2, and +1.5 $V_{RHE}$) at 10 mV s$^{-1}$. The second protocol consisted of two CVs starting at +0.05 $V_{RHE}$ and cycling to +1.2 $V_{RHE}$ UPL applying 2 mV s$^{-1}$ scan rate. Both protocols were ended with a potentiostatic hold for 3 to 5 min to allow the online ICP−MS signal to return to its baseline. Each protocol was conducted on a "fresh" catalyst spot in at least as a duplicate to test reproducibility.

**2.5. Physical Characterization.** Elemental composition of the electrocatalyst samples was studied with X-ray photoelectron spectroscopy (XPS). XPS survey spectra were recorded before and after electrochemical testing, using a Phi Quantera II X-ray scanning microprobe system. Spectra were recorded at a pass energy of 280 eV, a 0.5 eV step size, and 500 ms dwell time per step. The Al K$\alpha$ radiation (25 W, 15 kV) was focused on a 100 $\mu$m diameter spot on each sample. The resultant spectra were analyzed using the instrument-specific relative sensitivity factors in CasaXPS with a Shirley-type background of the Pt 4f and Ru 3p peaks.

Morphology of PtRu was mapped with scanning electron microscopy (SEM) before and after electrochemical testing. A Zeiss Crossbeam 540 Gemini II was operated at an accelerating voltage of 10 kV.

## 3. RESULTS

**3.1. Fundamental Electrochemical Behavior.** Compared to catalysts at fuel cell cathodes that experience high anodic potentials often, anode catalysts are unlikely to be exposed to potentials higher than +1.0 $V_{RHE}$. Still, the anode potential can be seriously increased at high loads, fuel starvation, and at the onset of the oxygen reduction reaction (ORR) during shutdown due to the presence of $O_2$ in the anode compartment. Information on the exact potentials during such cell reversal is limited, which implies that stability


https://dx.doi.org/10.1021/acscatal.0c02094
ACS Catal. 2020, 10, 10858−10870

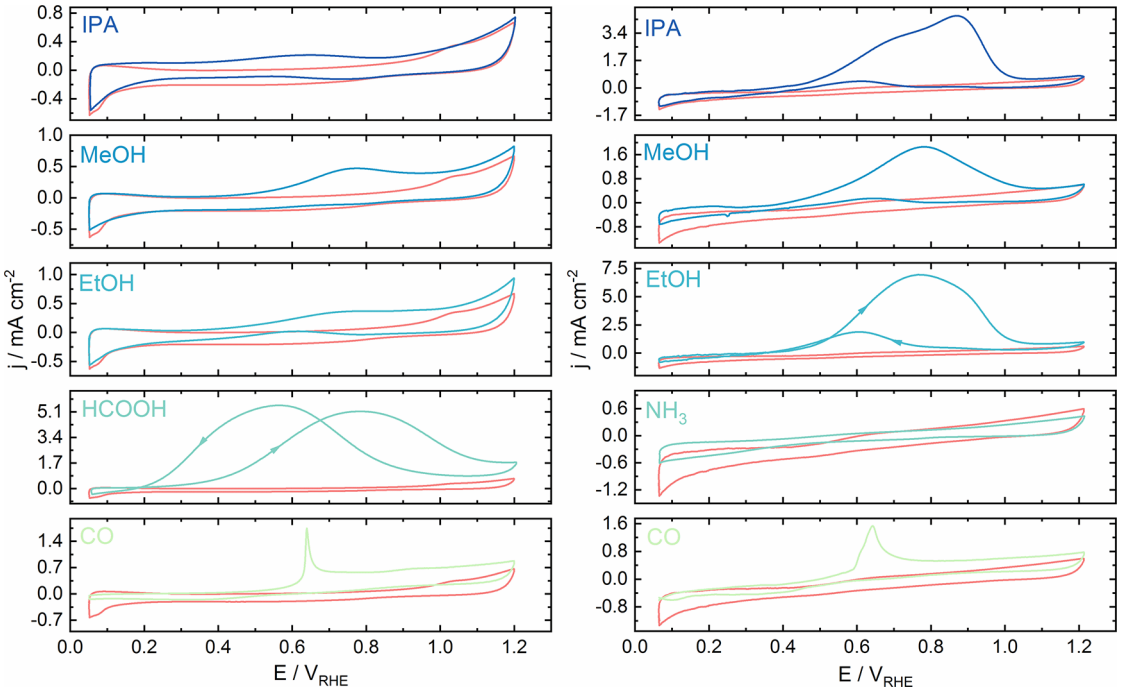


**Figure 1.** Cyclic voltammograms recorded for PtRu in 0.1 M $HClO_4$ (left) and in 0.05 M KOH (right) solutions and in the presence of various fuels applying 10 mV $s^{-1}$ scan rate. Data recorded for the blanks are presented in each graph (pale red curves). Electrolytes were saturated with Ar except in the case of CO.

must be studied in a broad potential window. Additionally, high anodic potentials are often used in numerous accelerated degradation protocols in fundamental studies.[37,38] Such potentials can result in the degradation of the catalyst layer through noble metal dissolution. Thus, the main goal of our work was to measure at which potentials can the dissolution of Pt and Ru be expected. First, to map the stability of PtRu in this potential regime, five CVs were recorded using +0.3 $V_{RHE}$, +0.6 $V_{RHE}$, +0.9 $V_{RHE}$, +1.2 $V_{RHE}$, and +1.5 $V_{RHE}$ as upper potential limits, applying 10 mV $s^{-1}$ scan rate. A set of CVs going to +1.2 $V_{RHE}$, recorded in 0.1 M $HClO_4$ and 0.05 M KOH with different fuels is presented in Figure 1. An increase in current can be observed on all CVs recorded in the presence of the various organics, corresponding to the electrocatalytic oxidation of the respective fuel. In the following, different phenomena observed on these CVs will be described more in detail.

In acidic medium (Figure 1, left), two anodic peaks can be identified in the presence of isopropanol compared to the blank, while only one peak is observed in the case of the methanol- and ethanol-containing solutions. The first, less intensive peak, appeared at an onset of ≈ +0.08 $V_{RHE}$, while the second one at ≈ +0.38 $V_{RHE}$. Only one peak is visible for methanol and ethanol with onsets at ≈ +0.29 $V_{RHE}$ and ≈ +0.25 $V_{RHE}$, respectively. These onsets are in line with previous literature results.[39] Two oxidation peaks in the presence of isopropanol were observed previously for PtRu/C microporous thin films,[40] and PtRu sputtered samples.[41] Since this phenomenon was seen only for PtRu alloys and not for their single-metal counterparts, the oxidation peak can be associated with the presence of Ru in the sample. The CV recorded in the HCOOH-containing electrolyte shows only one oxidation peak appeared at ≈ +0.20 $V_{RHE}$ onset potential, with a maximum current density of 5.1 mA $cm^{-2}$. This is ca. 1 order of magnitude higher than the ones obtained in the case of the alcohol-containing electrolytes. Data recorded for the CO-saturated electrolyte (in terms of the onset of oxidation and the overall shape) is similar to those collected during CO-stripping experiments, typically used for the determination of the electrochemically active surface area of Pt.[42−44] However, there is a significant difference in experimental conditions compared to such studies, namely: the electrolyte was constantly saturated with CO in our case. This resulted in higher anodic currents after the sharp oxidation peak thanks to the constant supply of CO adsorbing on the catalyst surface.

As for the CVs gathered in alkaline medium (Figure 1, right), significant differences can be seen compared to the acidic measurements. The current densities corresponding to alcohol oxidation are notably higher, also, the first of the two isopropanol oxidation peaks shifted toward more positive potentials and "blended in" the second peak. The onset potentials are close (∼+0.25 $V_{RHE}$) to the ones, determined from the CVs measured in $HClO_4$. Additionally, no electrocatalytic activity was observed toward the oxidation of $NH_3$. Indeed, the measured currents are even slightly smaller, compared to the blank curve. Finally, both in terms of the magnitude of the current density and the position of the oxidation peak, similar to in acidic pH electrolyte behavior was observed in the presence of CO.

### 3.2. Potential-Dependent Dissolution Rates of PtRu.

To gain insights on the stability of PtRu in the presence of the various fuels, the electrochemical cell was coupled to an inductively coupled mass spectrometer (online ICP−MS). In this way, the rate of both Pt and Ru dissolution can be tracked in real-time. To identify differences between fuels, measurements were also carried out in pure 0.1 M $HClO_4$ and 0.05 M KOH solutions. A slow potential scan was applied ($\upsilon$ = 10 mV $s^{-1}$) with a gradually increasing UPL from +0.3 $V_{RHE}$ up to +1.5 $V_{RHE}$ with 0.3 $V_{RHE}$ increments. Results, measured in 0.1 M $HClO_4$ are presented in Figure 2 (magnified data are shown


https://dx.doi.org/10.1021/acscatal.0c02094
ACS Catal. 2020, 10, 10858−10870

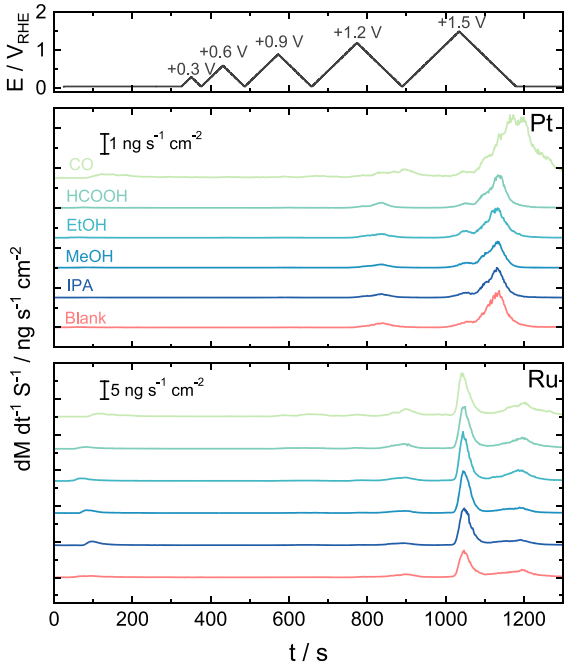


**Figure 2.** Dissolution rates of Pt and Ru for PtRu 1:1 catalyst recorded during a protocol consisting of five CVs with increasing upper potential limit from +0.3 $V_{RHE}$ to +1.5 $V_{RHE}$ ($\Delta E$ = 0.3 V, $\upsilon$ = 10 mV $s^{-1}$) in 0.1 M $HClO_4$ and in 0.1 M $HClO_4$+fuel solutions.

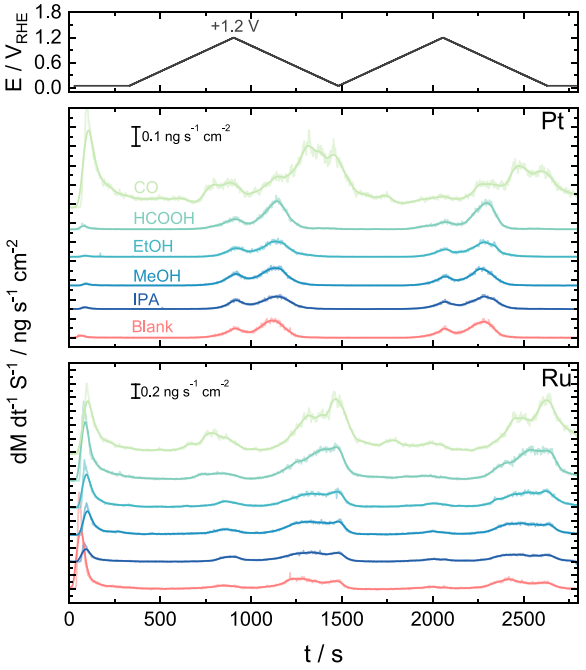


**Figure 3.** Dissolution rates of Pt and Ru for PtRu 1:1 catalyst recorded during a protocol consisting of two CVs from +0.05 $V_{RHE}$ to +1.2 $V_{RHE}$ applying 2 mV $s^{-1}$ scan rate in 0.1 M $HClO_4$ and 0.1 M $HClO_4$+fuel solution. The curves were smoothed using an FFT filter and only the smoothed data was processed further.

in Figure S1). First dissolution features are visible during the potentiostatic hold prior to recording the CVs. These emerged when the SFC got in contact with the working electrode. Transient Pt dissolution only starts during the forward scan of the fourth CV at +0.98 $V_{RHE}$, while transient Ru dissolution starts as low as +0.9 $V_{RHE}$. Onset potentials marking the start of dissolution, are summarized for all samples and protocols in Table S2. Both the anodic and cathodic dissolution increases if the UPL is higher (up to +1.5 $V_{RHE}$). However, the increase is more significant for the cathodic dissolution as it was already demonstrated for Pt in both acidic and alkaline electrolytes.[24] In the case of Ru, transient dissolution during the reverse scan can be already identified at UPL as low as +0.9 $V_{RHE}$ although, these signals are close to the baseline. Striking changes can be seen in dissolution rates if the UPL is +1.5 $V_{RHE}$: one additional peak appeared during the forward scan that is accompanied by the presence of two peaks during the reverse scan.

The dissolution features are qualitatively similar to the ones, measured for the blank in the presence of fuels. Both the onsets of dissolution and the shape of the dissolution peaks were unaffected by the addition of the fuels. The only exception is the dissolution of Pt if the solution was saturated with CO, in which case only cathodic dissolution occurred.

To make dissolution features more visible, an additional protocol was carried out applying 2 mV $s^{-1}$ scan rate. Two consecutive scans were recorded with the same UPL to see if dissolution changed after the first scan. The results are presented in Figure 3. For Pt, the two previously observed dissolution peaks are much better resolved at this slower scan rate. Apart from that, there are no differences occurred compared to the "faster" cycles. The picture is a bit different for Ru: four dissolution features are visible instead of three. Analogous to the data recorded applying 10 mV $s^{-1}$ scan rate, the presence of fuels did not change the rate of dissolution noticeably. Another important conclusion is that the dissolution features that appeared during the second scan are almost identical to the ones recorded during the first scan. Once again, the only exception to the previously described trends in the CO-containing electrolyte, in which several peaks appeared and the dissolution rates were visibly higher compared to the blank data.

Data collected for Pt and Ru dissolution in alkaline medium are similar to that obtained in acidic conditions both in terms of the onset of dissolution and the shape of the dissolution profiles (Figures S2 and S3). However, several differences can be identified: (i) the curves are noisier, (ii) the dissolution rates are significantly higher especially for Pt, and (iii) dissolution features are notably influenced by the presence of the various fuels. The noise originates from the fact that both the salts ($(NH_4)_2SO_4$ and KOH) and organics were applied in a concentration close to the limitations of the device. Dissolution rates measured for both metals are visibly higher compared to the data collected in acidic medium. According to precedent literature data,[22,24] at least approximately 4-times higher dissolution was expected for Pt (with +1.5 $V_{RHE}$ UPL). In contrast to this expectation, it can be already seen (qualitatively speaking) that the difference in our case is much higher. This experience can be explained by the fact that here the stability of an alloy was tested instead of its pure Pt counterpart, which can change the stability of both elements. This will be elaborated further in the discussion. Furthermore, only one anodic peak can be identified on the dissolution curves recorded during the forward scan, instead of the expected two.[24] The onset of dissolution has shifted to +1.05 − +1.1 $V_{RHE}$, while Ru dissolution only starts around +0.97 $V_{RHE}$, which is approximately 20 mV higher compared to the one,


https://dx.doi.org/10.1021/acscatal.0c02094
ACS Catal. 2020, 10, 10858−10870

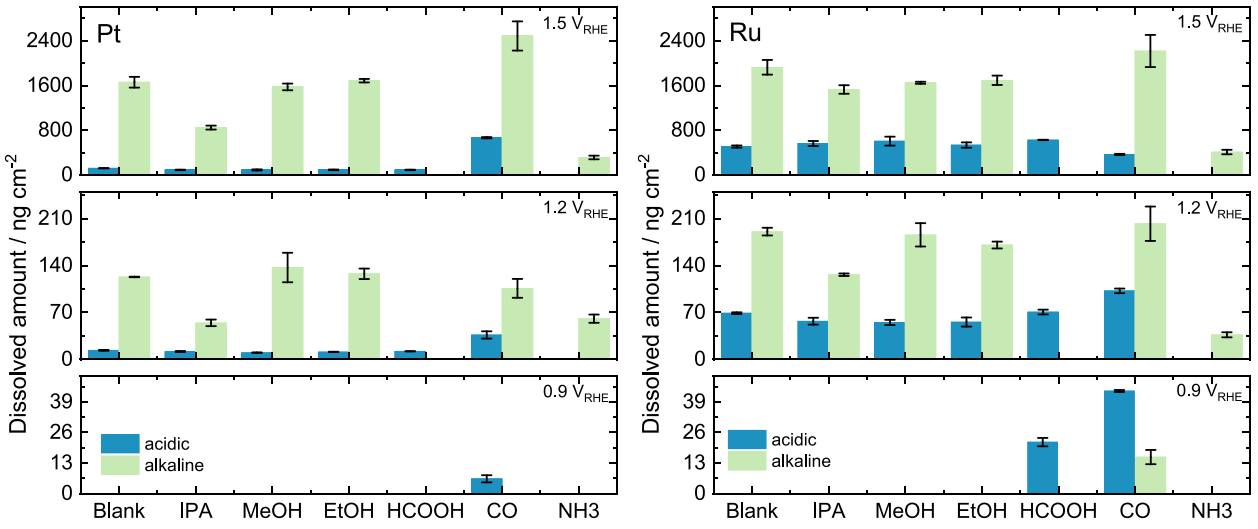


**Figure 4.** Dissolved amounts of Pt (left) and Ru (right) in the presence of various fuels both in 0.1 M $HClO_4$ and 0.05 M KOH solutions. The amounts of Pt and Ru dissolved were obtained by integrating the dissolution curves presented in Figures 2 and S2. Error bars were calculated from at least two measurements. Each measurement was performed on a fresh catalyst spot.

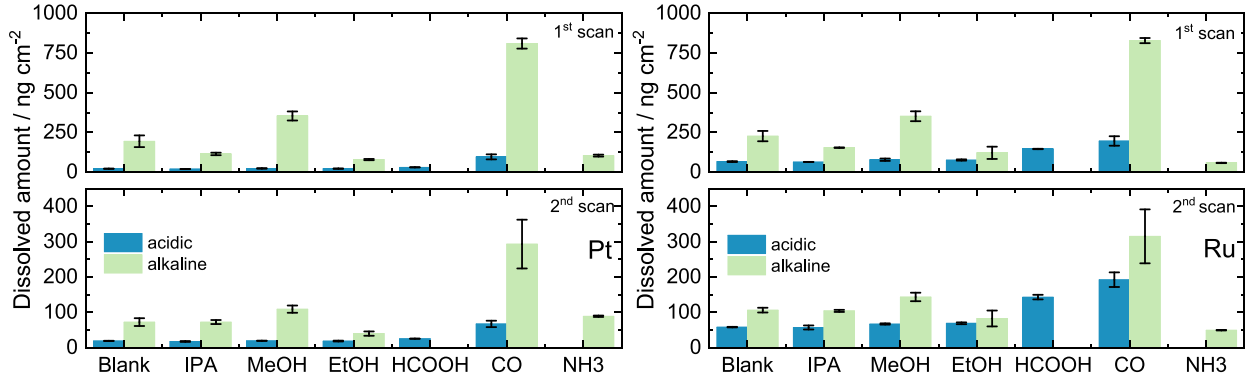


**Figure 5.** Dissolved amounts of Pt (left) and Ru (right) in the presence of various fuels both in 0.1 M $HClO_4$ and 0.05 M KOH solutions. The amounts of Pt and Ru dissolved were obained by integrating the dissolution curves presented in Figures 3 and S4. Error bars were calculated from at least two measurements. Each measurement was performed on a fresh catalyst spot.

determined in the acidic medium. Besides, there is no difference in the number of dissolution features if the UPL was kept at +1.2 $V_{RHE}$, but only one cathodic peak can be detected if the UPL was increased to +1.5 $V_{RHE}$.

Similar to the data, collected in acidic media, dissolution features in the presence of the various fuels are comparable to the ones obtained in 0.05 M KOH except for the case of the CO-saturated electrolyte. This applies both to the shape of the curves along with the onset of dissolution. However, notable differences in the magnitude of dissolution rates occurred upon addition of the fuels. It is the most pronounced in the case of isopropanol, in which a decreased dissolution of Pt and Ru was measured. Stability of both Pt and Ru seems to be similar in electrolytes with and without alcohols. The suppression of dissolution for both metals was also observed in the presence of $NH_3$, for which dissolution features almost "blend in" the baseline. The saturation of the electrolyte with CO resulted in enhanced Pt dissolution in parallel with the merging of the anodic and cathodic dissolution peaks, while Ru dissolution did not change visibly.

In the same way as in the case of 0.1 M $HClO_4$, data were also recorded applying 2 mV $s^{-1}$ scan rate in 0.05 M KOH based electrolytes (Figure S4). No additional peaks appeared on the recorded dissolution curves, however, measurement data were much noisier in alkaline media that makes the distinction of subtle changes challenging. This effect is especially strong in the presence of methanol, ethanol, and CO. Nevertheless, what one can conclude safely is that similar dissolution features can be identified as in the higher scan rate case. A further difference to the data acquired in acidic medium is that visibly less metals dissolved during the second cycle compared to the first one.

**3.3. Amounts of Pt and Ru Dissolution in Acidic and Alkaline Media.** To quantify the previously described qualitative observations, all dissolution curves were integrated. The amounts of dissolved metals, calculated from all data recorded applying 10 mV $s^{-1}$ scan rate both in acidic and alkaline media, are presented in Figure 4, while the ones obtained for the protocols carried out with 2 mV $s^{-1}$ scan rate are shown in Figure 5.



https://dx.doi.org/10.1021/acscatal.0c02094
ACS Catal. 2020, 10, 10858−10870

There is a huge difference between results calculated for the acidic and basic electrolytes. The amount of the dissolved Ru in pure alkaline media was 4-times higher, while a 14-fold increase was determined for Pt compared to the ones obtained for the acidic electrolyte. Additionally, the amount of Pt (e.g., in the blank measurement) was approximately 5-times less than the amount of Ru dissolved during potential cycling in 0.1 M $HClO_4$, while the quantity of the dissolved Pt and Ru was comparable in alkaline medium. The quantity of dissolved Pt and Ru calculated for the measurements performed with 2 mV $s^{-1}$ scan rate resulted in similar trends compared to data recorded at higher scan rates. Since two scans were recorded applying identical parameters it was possible to quantitatively study how the amount of dissolved metals changed after the first scan. It is visible that Pt and Ru dissolved in similar amount as during the first scan in acid. Contrastingly, as it has been already qualitatively concluded from Figure S4, much less Pt and Ru dissolved during the second scan in alkaline medium. This decrease was approximately 50%.

## 4. DISCUSSION

In the following, the effect of each fuel on the dissolution characteristics of PtRu is going to be discussed. Since the current work is a comparative study, the following discussion is by no means complete; further dedicated studies with each of the fuels will be required to obtain a more detailed understanding of PtRu stability in a given system. The discussion is divided into subsections adhering to the following criteria: dissolution characteristics experienced in the absence of fuels are discussed together, alcohols are discussed together, but to make statements more clear, data gathered for the acidic and alkaline media are discussed separately. Data collected in the presence of CO in acidic and alkaline media are presented together in a single subsection, while the effect of all the other fuels are discussed separately. Finally, the effect of dissolution on the surface composition of PtRu is added as a final section to highlight the extent of degradation.

**4.1. PtRu Dissolution in the Absence of Fuels.** The first visible feature on each dissolution curve, i.e., the contact peak, which corresponds to the reduction of the native oxides present on the surface of PtRu.[45] The observed scenario is similar to the one that occurs in a real device during start-up or after shutdown during which potential is left at rest due to the penetration of air into the anode side. This further justifies the need for measurements in an extended potential window since measuring the exact potential in such special cases is rather complicated. The onset potentials for Pt (Table S2) in acidic media (Figure 2) match with the oxidation potential calculated from thermodynamics (+0.98 $V_{RHE}$). The onset of dissolution for Pt in 0.05 M KOH (+1.10 $V_{RHE}$) is close to the one determined in 0.1 M $HClO_4$. The one for Ru (+0.97 $V_{RHE}$) is slightly higher than expected from the respective Pourbaix diagram (+0.74 $V_{RHE}$).[46] The dissolution rate of Ru in the PtRu alloy shows a different picture compared to the one measured previously for a Ru foil in alkaline media. While transient dissolution with observable dissolution peaks during the forward and reverse scan starting at +0.97 $V_{RHE}$ was observed for PtRu, Ru foil was dissolving constantly at high anodic potentials in the oxygen evolution reaction region.[22] However, it is important to note that our data were collected for an alloy in contrast to pristine metals, meaning that the presence of Pt might stabilize Ru. The difference between the onset potentials of dissolution determined for Pt and Ru proves that the online ICP−MS signals were originated from dissolution rather than the detachment of the catalyst layer. The onsets of the signals measured for Pt and Ru should be identical if particle detachment would be the major process.[47,48] The transient dissolution peak appeared around +0.95 $V_{RHE}$ corresponds to the reduction of the previously formed $PtO_x$ layer leading to higher dissolution rates compared to the forward scan.[37,46] Ru dissolution has already started during the reverse sweep of the third cycle (UPL = +0.9 $V_{RHE}$), originating from the reduction of various Ru oxide species (most likely $RuO_2{\cdot}2H_2O$ and $Ru(OH)_3$).[46] If the UPL was increased to +1.5 $V_{RHE}$, then an additional anodic peak appeared. This can be assigned to the formation of $RuO_4$, which is unstable causing enhanced Ru dissolution. The two cathodic peaks are corresponding to the reduction of $RuO_x$ to Ru, respectively. As it was mentioned above, trends in Pt dissolution were not altered when the scan rate was lowered to 2 mV $s^{-1}$ (Figure 3). Contrastingly, an additional dissolution peak is visible in the case of Ru. This fourth small peak appeared during the reverse scan and perhaps can be tied to the reduction of the surface oxides, however, it is hard to state the exact species judging from the thermodynamics. The peak corresponding to the reduction of $RuO_2{\cdot}2H_2O$ and $Ru(OH)_3$ to Ru might be separated due to the slower scan rate.

The amount of dissolved Pt and Ru calculated for the acidic and basic electrolytes (Figure 4 and 5) differed, namely, significantly more Ru and Pt dissolved in alkaline media. This indirectly shows that while much less Pt dissolved compared to the amount of Ru in 0.1 M $HClO_4$, the amount of Pt and Ru were comparable in 0.05 M KOH. If we take a closer look, these two observations are closely related. First of all, it has been already observed, that dissolution rates of Pt and Ru are notably higher in alkaline media. This behavior was attributed to the altered lifetime and amount of the formed metastable intermediates.[24] Such high increase in the dissolution of Pt was not expected since earlier studies on Pt showed only a 4-fold enhancement in basic electrolytes (if +1.5 $V_{RHE}$ UPL was applied).[24,37] In this case, however, the situation is a bit more complex, because of the presence of Ru atoms next to Pt since Ru is highly unstable especially in alkaline media due to the formation of $RuO_4^{2-}$ species causing severe dissolution.[22] As a consequence, the catalyst surface was locally destabilized due to the corrosion of Ru that in turn lead to significantly higher Pt dissolution.

**4.2. Effect of Alcohols on PtRu Dissolution in Acidic Media.** Pt dissolution in acidic media was less in the presence of all studied alcohols (applying 10 mV $s^{-1}$ scan rate), while Ru dissolution was less if the UPL was kept at +1.2 $V_{RHE}$, but identical to the blank at +1.5 $V_{RHE}$ UPL (Figure 4). To see the dissolved amount of Pt in the presence of alcohols better, magnified sections of Figures 4 and 5 are presented in the SI (Figure S5). The reason behind this decrease in the isopropanol-saturated electrolytes can be that the formed acetone[41,49] irreversibly adsorbs[50] on the catalyst surface, thus blocking it. As a result, less surface oxides dissolve during the reverse scan leading to decreased dissolution. This hypothesis was supported by recent results gathered with electrochemical real-time mass spectrometry (EC-RTMS)[51] and electrochemical infrared reflection absorption spectroscopy (EC-IRRAS).[52] The onset potential of acetone formation is approximately +0.05 $V_{RHE}$ on PtRu. Besides acetone the only detected product is $CO_2$, which forms with a gradually increasing amount above +0.8 $V_{RHE}$ UPL. As a result, the


https://dx.doi.org/10.1021/acscatal.0c02094
ACS Catal. 2020, 10, 10858−10870

poisoning effect of acetone is less pronounced at higher UPLs.[51,53] Higher dissolution rates were expected in the methanol-containing solutions suggested by the only study which we know of dealing with the stability of PtRu/C in the presence of methanol. The authors explained this with the adsorption of the formed CO intermediate on the catalyst surface facilitating the dissolution of PGMs.[35] We have also predicted this outcome based on our previous studies showing the effect of CO on dissolution characteristics of Pt.[32,35] However, an opposite effect was experienced since all three alcohols stabilized the surface, except for Ru with UPL = +1.5 $V_{RHE}$. Additionally, the stabilization effect decreased with increasing UPL. Our hypothesis is that at this high UPL $RuO_4$ forms, which is unstable leading to enhanced Ru dissolution. This effect overcompensates the stabilizing effect, caused by the adsorption of reaction intermediates. Differences between literature and our results might originate from the fact that a commercially available catalyst was employed in our study in contrast to a custom-synthesized one.

As for the stability of catalysts in the presence of ethanol, there was only one precedent study published.[54] This dealt with the stability of Janus-type carbon-supported Pt−$SnO_2$ electrocatalyst in the presence of ethanol in 0.1 M $HClO_4$. The effect of ethanol manifested in a lowered onset of dissolution (+0.57 $V_{RHE}$) and a significantly enhanced Pt dissolution in parallel with the appearance of a new dissolution peak. These findings contradict the ones in our study, but here it is important to note that the studied catalyst in that paper was not an alloy and that Sn is much less stable than Ru. According to the authors, the increased dissolution was explained with the Sn dissolution, which made more new Pt sites accessible to the electrolyte enhancing the corrosion of Pt. Additionally, the mechanism of ethanol oxidation proceeds differently on PtRu compared to Pt-$SnO_2$, namely: the $OH_{ad}$, formed on Ru can directly oxidize CO bound to Pt, while $OH_{ad}$ has to spill over to Pt to successfully oxidize CO in the case of Sn. The amount of dissolved Pt and Ru follows the same trends as in the case of methanol and isopropanol and can be explained similarly. The observed difference (lower dissolved amount of Pt and Ru in the presence of alcohols) is much smaller if the scan rate was decreased to 2 mV $s^{-1}$ (Figures 5 and S5). This effect probably occurred because the potential stayed for a longer period in a potential window in which neither Pt nor Ru is stable alleviating the previously described poisoning effect.

**4.3. Effect of Alcohols on PtRu Dissolution in Alkaline Media.** As for the total amount of Pt and Ru dissolved during the electrochemical protocol in alkaline media in the presence of the alcohols (results are shown in Figure 4) stabilizing effect was only observed upon the addition of isopropanol (20−30% less dissolution for Pt and 50% less for Ru compared to the blank). This decrease is more severe than it is in the acidic electrolyte. Contrastingly, there was not much of a change for methanol and ethanol. If we take a look at the total amount of the dissolved Pt and Ru calculated for the scans with 2 mV $s^{-1}$ scan rate (Figure S3), then the amount of Pt and Ru decreased in the presence of isopropanol and ethanol. However, the decrease in the case of isopropanol is less pronounced than in the case of the faster scans. Finally, the quantity of both noble metals notably increased if methanol was added to the electrolyte solution. Since we are not aware of any comprehensive reports on the stability of PGM alloys in alkaline media in the presence of either primary or secondary alcohols it is rather difficult to make solid conclusions for the experienced phenomena. The experienced increase in the dissolution of both Pt and Ru in the methanol-containing electrolyte at the slower scan rate might root in the fact that the system stayed much longer at potentials at which both Pt and Ru are unstable resulting in increased dissolution. Although, if this is the case, then higher PGM dissolution should have occurred in the presence of ethanol as well, which contradicts our measurement data. Similar to the acidic electrolyte, the decrease of dissolution in isopropanol-containing solutions can be due to the altered adsorption/desorption characteristics of acetone from the catalyst surface. However, here it seems that the main oxidation product is still acetone and not $CO_2$ as it was in the acidic electrolyte resulting in lower dissolution even at the highest applied UPL.

**4.4. Effect of Formic Acid on PtRu Dissolution in Acidic Media.** Dissolution characteristics (in terms of the amount of the dissolved metals) were not influenced strikingly by the presence of formic acid if the scan rate was 10 mV $s^{-1}$. There was only a slight increase in Ru dissolution (20%) accompanied by 25% less Pt dissolution at the highest UPL. However, at 2 mV $s^{-1}$ scan rate, 50% and 100% more Pt and Ru dissolved compared to the blank sample. The electro-oxidation of formic acid can proceed via three pathways: (i) direct pathway, where formic acid is directly oxidized to $CO_2$, (ii) indirect pathway, where the adsorbed formic acid gets dehydrated, forming adsorbed CO which is oxidized to $CO_2$ in a subsequent step, and (iii) the formate pathway, where first an adsorbed formate forms, which is oxidized to $CO_2$ in a separate step.[55,56] The role of Ru in the PtRu alloy is to supply O atoms in the form of adsorbed hydroxide, thus suppressing the formation of CO, which otherwise would block the surface of Pt.[56,57] However, it seems that if the scan rate is high enough, formic acid had little influence on dissolution properties of PtRu, while visible changes occurred if the scan rate was 2 mV $s^{-1}$. This observation is rather similar to the one, made in the case of alcohols, thus results can be explained similarly; either more $CO_{ad}$ forms due to the lower scan rate,[23] and/or the potential stays longer in the potential-window in which neither Pt nor Ru are stable. Similar effects of formic acid on catalyst stability were observed in a previous study performed on Pt ultrathin films grown on Au by surface limited redox replacement of an underpotentially deposited Pb layer. An approximately 4−5-times higher Pt dissolution was experienced in the presence of formic acid, which is much higher than the ones calculated for Pt in our case.[58] This difference might be explained by the different parameters used in this study: there, only Pt was applied as the catalyst, measurement of Pt dissolution was performed ex-situ and the scan rate and UPL were different (UPL was as high as the onset of Pt dissolution). In general, to see if Ru has any effect on the stability of PtRu and to identify the processes behind the experienced increase in dissolution at slow scan rates, more detailed investigations has to be carried out on PtRu alloys with varying Ru content in catalyst and formic acid in electrolyte.

**4.5. Effect of Ammonia on PtRu Dissolution in Alkaline Media.** Results gathered in the presence of ammonia are rather interesting since, as it was presented in Figure 1, PtRu seems to be inactive toward the electrocatalytic oxidation of ammonia. The calculated amounts of Pt and Ru showed a strong stabilization of the alloy since approximately 2−5-times less Pt and 5-times less Ru dissolved from the catalyst surface if the electrolyte contained ammonia (10 mV $s^{-1}$ scan rate,


https://dx.doi.org/10.1021/acscatal.0c02094
ACS Catal. 2020, 10, 10858−10870

Figure 4). It is well-known that $NH_3$ and $NO_2^-$ can form thermodynamically stable complexes with PGMs (e.g., $[Pt(NH_3)_4]^{2+}$)[59,60] at this pH, which can modify, for example, the redeposition of Pt and Ru. However, the effect of complex formation should be an increase in dissolution. According to our data, this scenario does not play a notable role in the dissolution characteristics in the presence of ammonia. The origin of a decrease in dissolution for both metals perhaps is the adsorption of $NH_x$ and $NO_x$ species on the catalyst, which leads to the passivation of the surface and in the end to the formation of less oxides. The presence of such intermediates on the surface of Pt was proven by EC-RTMS[61] and in situ infrared spectroscopy.[61,62] Similar behavior was seen for Pt in the presence of *small amounts* of $Cl^-$ ions.[12] Both the activity (CVs) and stability data implies that the adsorption of these intermediates on the surface of PtRu is irreversible in the potential window of our investigations. Again, it is important to note here that it is impossible to make solid explanations because the literature lacks reports on the stability of PGMs and their alloys in the presence of ammonia accompanied by detailed studies in which each intermediate is carefully identified. Therefore, it is not known if the seen effect would be the same if the studied material is active in the electrocatalytic ammonia oxidation reaction. To crack this mystery, similar steps have to be made as in the formic acid-case.

**4.6. Effect of CO on PtRu Dissolution in Acidic and Alkaline Media.** The amount of Pt dissolved has increased by about 2.4- and 5-times in 0.1 M $HClO_4$ saturated with CO applying +1.2 $V_{RHE}$ and +1.5 $V_{RHE}$ UPL, respectively. Contrastingly, the amount of Ru was only increased by 1.5 times, but if the UPL was increased to the most positive value Ru dissolution was notably decreased by 1.4 times. Moreover, CO was the only fuel in which presence the onset of dissolution for both Pt and Ru shifted toward less negative potentials (+0.86 $V_{RHE}$ for Pt and +0.67 $V_{RHE}$ for Ru). According to the determined dissolved amounts, it seems that the presence of CO had a much bigger influence on the stability of the Pt counterpart. This may have emerged because the mode and energy of CO adsorption is different on Ru as it has been already proposed by many other reports in the literature.[63−66] In the case of the measurements performed applying 2 mV $s^{-1}$ scan rate the differences compared to the blank are doubled (5-times more Pt and 3-times more Ru dissolved) meaning that the scan rate has a key effect on dissolution characteristics in the presence of CO. In contrast to the measurements in 0.1 M $HClO_4$, only negligible changes were observed compared to the blank in the CO-saturated 0.05 M KOH solution. Although if the scan rate was 2 mV $s^{-1}$, 4-times more Pt and 3.6-times more Ru dissolved suggesting that the scan rate had an even bigger effect on dissolution compared to the acidic case. The increase in dissolution in the presence of CO was already reported for pure Pt electrodes, which was attributed to the blockage of the Pt surface toward oxidation (this is why there is very little anodic dissolution), and also blocking the reduced Pt sites during the reverse scan prevented the redeposition of Pt on these sites.[23] The two processes combined resulted in enhanced dissolution.

Here we also have to briefly explain the experienced difference in the dissolution of Pt and Ru in between the alcohol-, HCOOH-, and CO-containing electrolytes. The common thread in these systems is the presence of $CO_{ad}$ on the surface of PtRu. However, significantly higher dissolved amounts were measured if the electrolyte was saturated with CO (see the explanation above). It has been shown by surface-enhanced infrared absorption spectroscopy (SEIRAS) measurements that $CO_{ad}$ can only be detected below ∼+0.6 $V_{RHE}$ (PtRu/C, methanol oxidation) and below ∼+0.8 $V_{RHE}$ (Pt/C, methanol, and HCOOH oxidation).[67−70] The amount of $CO_{ad}$ starts to rapidly decrease above the onset potential of oxidation of the respective fuel. This means that there is no $CO_{ad}$ present at the potential window in which Pt and Ru are unstable. Contrastingly, if the electrolyte is saturated with CO, there is a constant supply of CO even at these relatively high potentials, which can adsorb on the electrocatalyst surface facilitating its dissolution.

A tremendous amount of studies were published on the electrocatalytic oxidation of CO either in acidic[42,43] or alkaline[71−73] media. According to these, several factors can influence this process for example: first, to oxidize CO on the PGM it is necessary to have oxygenated species adsorbed on the surface in close proximity to the adsorbed CO, which will donate O atoms. In an acidic environment, the formation of such species occurs through the activation of adsorbed water (which predominantly takes place on Ru in PtRu alloys), while in alkaline solutions these are mostly $OH^-$ ions adsorbed from the surrounding electrolyte.[73] Additionally, the presence of different cations ($K^+$ vs $H^+$) can also influence activity.[72] Finally, it has also been proposed that on pure Pt(111) and Pt(111)Ru alloy the mechanism of the electrocatalytic oxidation of CO in alkaline media proceeds via either a Rideal−Eley or a mixed Rideal−Eley and Langmuir−Hinshelwood mechanism as opposed to acidic pH, at which the reaction follows a Langmuir−Hinshelwood mechanism.[71] It can easily be seen that factors influencing the electrocatalytic activity can also affect the stability of PtRu, and thus the observed dissolution characteristics.

**4.7. Effect of Dissolution on the Composition of PtRu.** To see how dissolution alters the surface composition and morphology of the catalyst XPS and SEM measurements were conducted. First, the composition of the electrocatalyst *after* performing the electrochemical protocol (five consecutive CVs with gradually increasing UPL from +0.3 $V_{RHE}$ to +1.5 $V_{RHE}$ with $\Delta E$ = 0.3 V applying 10 mV $s^{-1}$ scan rate) was calculated. Figure 6 shows the Ru content of the samples compared to the

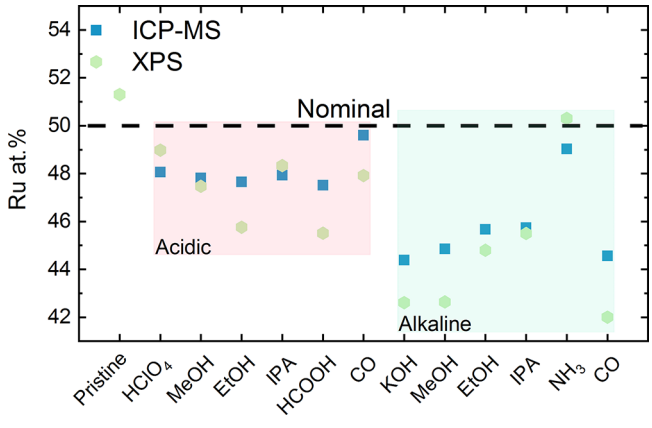


**Figure 6.** Ru content of PtRu before (pristine) and after performing the electrochemical protocol both in the absence and presence of fuels. The electrochemical protocol consisted of five subsequent CVs with gradually increasing UPL starting from +0.3 $V_{RHE}$ to +1.5 $V_{RHE}$ ($\Delta E$ = 0.3 V) applying 10 mV $s^{-1}$ scan rate.


https://dx.doi.org/10.1021/acscatal.0c02094
ACS Catal. 2020, 10, 10858−10870

nominal composition before ("pristine") and after the electrochemical protocols both in the absence and in the presence of fuels. Survey XPS spectra (Figure S6) were recorded from PtRu before and after electrochemical testing both in acidic and alkaline media. It is visible that according to the XPS data, the Ru content is almost identical to the nominal composition provided by the manufacturer in the pristine sample. The most important conclusion here is that the XPS data nicely reflect the trends already observed from the ICP−MS measurements. It matches well with the PtRu compositions calculated from the dissolved amounts (see Figures 4 and 5). The Pt/Ru ratio only slightly changes in acidic media, while this change in composition is much higher in alkaline media. The only exception is when $NH_3$ is present in the solution; here the Ru content is identical to the nominal value. The highest change in composition occurred in 0.05 M KOH (~42.6 at% Ru) and when it was saturated with CO (~42 at% Ru).

The change in morphology after the electrochemical protocols was mapped with SEM (Figures S7 and S8). It is important to note here that the magnification of our SEM images allows only qualitative comparison. The PtRu nanoparticles can be observed as small bright spots sitting on the underlying nanocarbon particles. Additionally, the nanocarbon support did not corrode upon applying the electrochemical protocol (samples are identical to the ones used during the XPS measurements), it retained its original morphology. The same applies to the PtRu nanoparticles in acidic media: all SEM images are identical to the one that was collected from the pristine sample. However, there are visible changes that can be discovered in the case of the samples tested in alkaline media: the number of PtRu nanoparticles is lower but their size is notably bigger compared to the pristine PtRu sample. The only exception is when $NH_3$ was the fuel, in which case the morphology of the electrocatalyst occurs similar to that of the pristine PtRu sample. In conclusion, the observed morphological changes are in line with the online ICP−MS and XPS results.

## 5. CONCLUSIONS

The influence of various fuels on the stability of carbon-supported PtRu was studied with online ICP−MS. It was identified that the dissolution of Pt and Ru starts at +0.98 $V_{RHE}$ and +0.81 $V_{RHE}$, respectively. This implies that during regular operation within the typical range of a fuel cell anode, dissolution is not crucial. Hence, so far reported stability issues of PGM catalysts below +0.8 $V_{RHE}$ can, therefore, be traced back to other degradation mechanisms (e.g., particle detachment, surface atom rearrangement, poisoning, etc.).[14,56,74,75] The onset potential of dissolution for both Pt and Ru was not affected by the presence of fuels (the only exception is CO in acidic medium where both metals started to dissolve at approximately 130−140 mV lower positive potentials). In general, while the onset of PtRu dissolution is similar in all electrolytes, stability in alkaline media was significantly lower regardless of the presence of any fuel. Although it is important to note that the onset of dissolution was not shifted notably by changing the pH from acidic to alkaline. Transferring these new findings to the practical application of PtRu/C in fuel cells we suggest that, to make sure that performance losses are not originating from the dissolution of the catalyst layer, all experiments probing both the activity and the stability of the given catalyst should be designed in a manner to stay below the reported dissolution potentials. Additionally, it also needs to be carefully investigated if there are any events that occur (e.g., crossover of $O_2$ from the cathode side), which increases the OCV up to a point where the dissolution of Pt and especially Ru can take place. Presently, this is especially important since one major intention is to lower the PGM content of catalyst layers as much as possible. Therefore, any loss of catalyst and a decrease in Ru surface concentration would seriously affect device performance. Finally, it is important to underline that observations and conclusions are based on experiments using rather low fuel concentrations. Studies performed with higher fuel concentrations and measurements with other in situ techniques are planned in the future to precisely identify the intermediates present on the catalyst surface and to better understand factors influencing the stability of PtRu.

## ■ ASSOCIATED CONTENT

### Supporting Information

The Supporting Information is available free of charge at https://pubs.acs.org/doi/10.1021/acscatal.0c02094.

Additional experimental details, the onset potentials of dissolution in the presence of the various fuels, additional dissolution data in acidic and alkaline media, XPS data, and SEM images before and after performing electrochemical protocols (PDF)

## ■ AUTHOR INFORMATION


### Corresponding Authors

**Attila Kormányos** − *Helmholtz-Institute Erlangen-Nürnberg for Renewable Energy (IEK-11), Forschungszentrum Jülich, 91058 Erlangen, Germany;* orcid.org/0000-0002-2145-7419; Email: a.kormanyos@fz-juelich.de, @attilakormanyos

**Serhiy Cherevko** − *Helmholtz-Institute Erlangen-Nürnberg for Renewable Energy (IEK-11), Forschungszentrum Jülich, 91058 Erlangen, Germany*; Email: s.cherevko@fz-juelich.de, @CherevkoSerhiy

### Authors

**Florian D. Speck** − *Helmholtz-Institute Erlangen-Nürnberg for Renewable Energy (IEK-11), Forschungszentrum Jülich, 91058 Erlangen, Germany; Department of Chemical and Biological Engineering, Friedrich-Alexander-Universität Erlangen-Nürnberg, 91058 Erlangen, Germany;* orcid.org/0000-0002-7649-9261

**Karl J. J. Mayrhofer** − *Helmholtz-Institute Erlangen-Nürnberg for Renewable Energy (IEK-11), Forschungszentrum Jülich, 91058 Erlangen, Germany; Department of Chemical and Biological Engineering, Friedrich-Alexander-Universität Erlangen-Nürnberg, 91058 Erlangen, Germany*

Complete contact information is available at: https://pubs.acs.org/10.1021/acscatal.0c02094


### Notes

The authors declare no competing financial interest.

## ■ ACKNOWLEDGMENTS

This work was funded by the Bavarian Ministry of Economic Affairs, Regional Development and Energy. The authors would like to thank Markus Bierling for his help during the SEM measurements. We thank the four anonymous reviewers for their constructive criticism of the earlier version of our manuscript.

## REFERENCES


(1) Møller, K. T.; Jensen, T. R.; Akiba, E.; Li, H.-w. Hydrogen - A sustainable energy carrier. *Prog. Nat. Sci.* **2017**, *27* (1), 34−40.

(2) Preuster, P.; Alekseev, A.; Wasserscheid, P. Hydrogen Storage Technologies for Future Energy Systems. *Annu. Rev. Chem. Biomol. Eng.* **2017**, *8*, 445−471.

(3) Lamy, C.; Lima, A.; LeRhun, V.; Delime, F.; Coutanceau, C.; Léger, J.-M. Recent advances in the development of direct alcohol fuel cells (DAFC). *J. Power Sources* **2002**, *105* (2), 283−296.

(4) Zhang, J.; Chen, M.; Li, H.; Li, Y.; Ye, J.; Cao, Z.; Fang, M.; Kuang, Q.; Zheng, J.; Xie, Z. Stable palladium hydride as a superior anode electrocatalyst for direct formic acid fuel cells. *Nano Energy* **2018**, *44*, 127−134.

(5) Gottesfeld, S. The Direct Ammonia Fuel Cell and a Common Pattern of Electrocatalytic Processes. *J. Electrochem. Soc.* **2018**, *165* (15), J3405−J3412.

(6) Suzuki, S.; Muroyama, H.; Matsui, T.; Eguchi, K. Fundamental studies on direct ammonia fuel cell employing anion exchange membrane. *J. Power Sources* **2012**, *208*, 257−262.

(7) Velázquez-Palenzuela, A.; Centellas, F.; Garrido, J. A.; Arias, C.; Rodríguez, R. M.; Brillas, E.; Cabot, P.-L. Kinetic analysis of carbon monoxide and methanol oxidation on high performance carbon-supported Pt−Ru electrocatalyst for direct methanol fuel cells. *J. Power Sources* **2011**, *196* (7), 3503−3512.

(8) Garg, A.; Milina, M.; Ball, M.; Zanchet, D.; Hunt, S. T.; Dumesic, J. A.; Roman-Leshkov, Y. Transition-Metal Nitride Core@ Noble-Metal Shell Nanoparticles as Highly CO Tolerant Catalysts. *Angew. Chem., Int. Ed.* **2017**, *56* (30), 8828−8833.

(9) Liu, J.; Lucci, F. R.; Yang, M.; Lee, S.; Marcinkowski, M. D.; Therrien, A. J.; Williams, C. T.; Sykes, E. C.; Flytzani-Stephanopoulos, M. Tackling CO Poisoning with Single-Atom Alloy Catalysts. *J. Am. Chem. Soc.* **2016**, *138* (20), 6396−9.

(10) Sievi, G.; Geburtig, D.; Skeledzic, T.; Bösmann, A.; Preuster, P.; Brummel, O.; Waidhas, F.; Montero, M. A.; Khanipour, P.; Katsounaros, I.; Libuda, J.; Mayrhofer, K. J. J.; Wasserscheid, P. Towards an efficient liquid organic hydrogen carrier fuel cell concept. *Energy Environ. Sci.* **2019**, *12* (7), 2305−2314.

(11) Müller, K.; Stark, K.; Emel'yanenko, V. N.; Varfolomeev, M. A.; Zaitsau, D. H.; Shoifet, E.; Schick, C.; Verevkin, S. P.; Arlt, W. Liquid Organic Hydrogen Carriers: Thermophysical and Thermochemical Studies of Benzyl- and Dibenzyl-toluene Derivatives. *Ind. Eng. Chem. Res.* **2015**, *54* (32), 7967−7976.

(12) Geiger, S.; Cherevko, S.; Mayrhofer, K. J. J. Dissolution of Platinum in Presence of Chloride Traces. *Electrochim. Acta* **2015**, *179*, 24−31.

(13) Chen, W.; Sun, G.; Liang, Z.; Mao, Q.; Li, H.; Wang, G.; Xin, Q.; Chang, H.; Pak, C.; Seung, D. The stability of a PtRu/C electrocatalyst at anode potentials in a direct methanol fuel cell. *J. Power Sources* **2006**, *160* (2), 933−939.

(14) Antolini, E. The problem of Ru dissolution from Pt−Ru catalysts during fuel cell operation: analysis and solutions. *J. Solid State Electrochem.* **2011**, *15* (3), 455−472.

(15) Liu, J.; Zhou, Z.; Zhao, X.; Xin, Q.; Sun, G.; Yi, B. Studies on performance degradation of a direct methanol fuel cell (DMFC) in life test. *Phys. Chem. Chem. Phys.* **2004**, *6* (1), 134.

(16) Uhm, S.; Lee, J. Accelerated durability test of DMFC electrodes by electrochemical potential cycling. *J. Ind. Eng. Chem.* **2009**, *15* (5), 661−664.

(17) Jing, F.; Sun, R.; Wang, S.; Sun, H.; Sun, G. Effect of the Anode Structure on the Stability of a Direct Methanol Fuel Cell. *Energy Fuels* **2020**, *34* (3), 3850−3857.

(18) Park, G.-S.; Pak, C.; Chung, Y.-S.; Kim, J.-R.; Jeon, W. S.; Lee, Y.-H.; Kim, K.; Chang, H.; Seung, D. Decomposition of Pt−Ru anode catalysts in direct methanol fuel cells. *J. Power Sources* **2008**, *176* (2), 484−489.

(19) Pizzutilo, E.; Freakley, S. J.; Geiger, S.; Baldizzone, C.; Mingers, A.; Hutchings, G. J.; Mayrhofer, K. J. J.; Cherevko, S. Addressing stability challenges of using bimetallic electrocatalysts: the case of gold−palladium nanoalloys. *Catal. Sci. Technol.* **2017**, *7* (9), 1848−1856.

(20) Cherevko, S.; Keeley, G. P.; Geiger, S.; Zeradjanin, A. R.; Hodnik, N.; Kulyk, N.; Mayrhofer, K. J. Dissolution of Platinum in the Operational Range of Fuel Cells. *ChemElectroChem* **2015**, *2* (10), 1471−1478.

(21) Cherevko, S.; Geiger, S.; Kasian, O.; Kulyk, N.; Grote, J.-P.; Savan, A.; Shrestha, B. R.; Merzlikin, S.; Breitbach, B.; Ludwig, A.; Mayrhofer, K. J. J. Oxygen and hydrogen evolution reactions on Ru, $RuO_2$, Ir, and $IrO_2$ thin film electrodes in acidic and alkaline electrolytes: A comparative study on activity and stability. *Catal. Today* **2016**, *262*, 170−180.

(22) Schalenbach, M.; Kasian, O.; Ledendecker, M.; Speck, F. D.; Mingers, A. M.; Mayrhofer, K. J. J.; Cherevko, S. The Electrochemical Dissolution of Noble Metals in Alkaline Media. *Electrocatalysis* **2018**, *9* (2), 153−161.

(23) Topalov, A. A.; Zeradjanin, A. R.; Cherevko, S.; Mayrhofer, K. J. J. The impact of dissolved reactive gases on platinum dissolution in acidic media. *Electrochem. Commun.* **2014**, *40*, 49−53.

(24) Cherevko, S.; Zeradjanin, A. R.; Keeley, G. P.; Mayrhofer, K. J. J. A Comparative Study on Gold and Platinum Dissolution in Acidic and Alkaline Media. *J. Electrochem. Soc.* **2014**, *161* (12), H822−H830.

(25) Hornberger, E.; Bergmann, A.; Schmies, H.; Kühl, S.; Wang, G.; Drnec, J.; Sandbeck, D. J. S.; Ramani, V.; Cherevko, S.; Mayrhofer, K. J. J.; Strasser, P. In Situ Stability Studies of Platinum Nanoparticles Supported on Ruthenium−Titanium Mixed Oxide (RTO) for Fuel Cell Cathodes. *ACS Catal.* **2018**, *8* (10), 9675−9683.

(26) Geiger, S.; Kasian, O.; Ledendecker, M.; Pizzutilo, E.; Mingers, A. M.; Fu, W. T.; Diaz-Morales, O.; Li, Z.; Oellers, T.; Fruchter, L.; Ludwig, A.; Mayrhofer, K. J. J.; Koper, M. T. M.; Cherevko, S. The stability number as a metric for electrocatalyst stability benchmarking. *Nat. Catal.* **2018**, *1* (7), 508−515.

(27) Cherevko, S. Stability and dissolution of electrocatalysts: Building the bridge between model and "real world" systems. *Curr. Opin. Electrochem.* **2018**, *8*, 118−125.

(28) Kasian, O.; Geiger, S.; Mayrhofer, K. J. J.; Cherevko, S. Electrochemical On-line ICP-MS in Electrocatalysis Research. *Chem. Rec.* **2019**, *19* (10), 2130−2142.

(29) Watanabe, M.; Motoo, S. Electrocatalysis by ad-atoms: Part II. Enhancement of the oxidation of methanol on platinum by ruthenium ad-atoms. *J. Electroanal. Chem. Interfacial Electrochem.* **1975**, *60* (3), 267−273.

(30) Sacré, N.; Duca, M.; Garbarino, S.; Imbeault, R.; Wang, A.; Hadj Youssef, A.; Galipaud, J.; Hufnagel, G.; Ruediger, A.; Roué, L.; Guay, D. Tuning Pt−Ir Interactions for $NH_3$ Electrocatalysis. *ACS Catal.* **2018**, *8* (3), 2508−2518.

(31) Joo, J.; Uchida, T.; Cuesta, A.; Koper, M. T.; Osawa, M. Importance of acid-base equilibrium in electrocatalytic oxidation of formic acid on platinum. *J. Am. Chem. Soc.* **2013**, *135* (27), 9991−4.

(32) Hodnik, N.; Baldizzone, C.; Polymeros, G.; Geiger, S.; Grote, J. P.; Cherevko, S.; Mingers, A.; Zeradjanin, A.; Mayrhofer, K. J. Platinum recycling going green via induced surface potential alteration enabling fast and efficient dissolution. *Nat. Commun.* **2016**, *7* (1), 13164.

(33) Santasalo-Aarnio, A.; Tuomi, S.; Jalkanen, K.; Kontturi, K.; Kallio, T. The correlation of electrochemical and fuel cell results for alcohol oxidation in acidic and alkaline media. *Electrochim. Acta* **2013**, *87*, 730−738.

(34) Antolini, E. Effect of the structural characteristics of binary Pt-Ru and ternary Pt-Ru-M fuel cell catalysts on the activity of ethanol electrooxidation in acid medium. *ChemSusChem* **2013**, *6* (6), 966−73.

(35) Jovanovič, P.; Šelih, V. S.; Šala, M.; Hočevar, S.; Ruiz-Zepeda, F.; Hodnik, N.; Bele, M.; Gaberšček, M. Potentiodynamic dissolution study of PtRu/C electrocatalyst in the presence of methanol. *Electrochim. Acta* **2016**, *211*, 851−859.

(36) Sebastián, D.; Stassi, A.; Siracusano, S.; Vecchio, C. L.; Aricò, A. S.; Baglio, V. Influence of Metal Oxide Additives on the Activity and Stability of PtRu/C for Methanol Electro-Oxidation. *J. Electrochem. Soc.* **2015**, *162* (7), F713−F717.




https://dx.doi.org/10.1021/acscatal.0c02094
ACS Catal. 2020, 10, 10858−10870

(37) Cherevko, S. *Electrochemical Dissolution of Noble Metals*; Elsevier: Edinburgh, 2018.
(38) Hodnik, N.; Jovanovič, P.; Pavlišič, A.; Jozinović, B.; Zorko, M.; Bele, M.; Šelih, V. S.; Šala, M.; Hočevar, S.; Gaberšček, M. New Insights into Corrosion of Ruthenium and Ruthenium Oxide Nanoparticles in Acidic Media. *J. Phys. Chem. C* **2015**, *119* (18), 10140−10147.
(39) Santasalo-Aarnio, A.; Borghei, M.; Anoshkin, I. V.; Nasibulin, A. G.; Kauppinen, E. I.; Ruiz, V.; Kallio, T. Durability of different carbon nanomaterial supports with PtRu catalyst in a direct methanol fuel cell. *Int. J. Hydrogen Energy* **2012**, *37* (4), 3415−3424.
(40) Lee, C.-G.; Umeda, M.; Uchida, I. Cyclic voltammetric analysis of C1−C4 alcohol electrooxidations with Pt/C and Pt−Ru/C microporous electrodes. *J. Power Sources* **2006**, *160* (1), 78−89.
(41) Lee, C.-G.; Ojima, H.; Umeda, M. Electrooxidation of C1 to C3 alcohols with Pt and Pt−Ru sputter deposited interdigitated array electrodes. *Electrochim. Acta* **2008**, *53* (7), 3029−3035.
(42) Wang, K.; Gasteiger, H. A.; Markovic, N. M.; Ross, P. N. On the reaction pathway for methanol and carbon monoxide electrooxidation on Pt-Sn alloy versus Pt-Ru alloy surfaces. *Electrochim. Acta* **1996**, *41* (16), 2587−2593.
(43) Gasteiger, H. A.; Markovic, N.; Ross, P. N.; Cairns, E. J. Carbon monoxide electrooxidation on well-characterized platinum-ruthenium alloys. *J. Phys. Chem.* **1994**, *98* (2), 617−625.
(44) Jiang, J.; Kucernak, A. Electrooxidation of small organic molecules on mesoporous precious metal catalysts. *J. Electroanal. Chem.* **2003**, *543* (2), 187−199.
(45) Cherevko, S. Electrochemical dissolution of noble metals native oxides. *J. Electroanal. Chem.* **2017**, *787*, 11−13.
(46) Pourbaix, M. *Atlas of Electrochemical Equilibria in Aqueous Solutions*; 1974.
(47) Lafforgue, C.; Chatenet, M.; Dubau, L.; Dekel, D. R. Accelerated Stress Test of Pt/C Nanoparticles in an Interface with an Anion-Exchange Membrane—An Identical-Location Transmission Electron Microscopy Study. *ACS Catal.* **2018**, *8* (2), 1278−1286.
(48) Lafforgue, C.; Maillard, F.; Martin, V.; Dubau, L.; Chatenet, M. Degradation of Carbon-Supported Platinum-Group-Metal Electrocatalysts in Alkaline Media Studied by in Situ Fourier Transform Infrared Spectroscopy and Identical-Location Transmission Electron Microscopy. *ACS Catal.* **2019**, *9* (6), 5613−5622.
(49) Rodrigues, I. d. A.; De Souza, J. P. I.; Pastor, E.; Nart, F. C. Cleavage of the C−C Bond during the Electrooxidation of 1-Propanol and 2-Propanol: Effect of the Pt Morphology and of Codeposited Ru. *Langmuir* **1997**, *13* (25), 6829−6835.
(50) Wieckowski, A.; Zelenay, P.; Szklarczyk, M.; Sobkowski, J. The Pt-acetone-water system investigated by radiotracer and electrochemical methods. *J. Electroanal. Chem. Interfacial Electrochem.* **1982**, *135* (2), 285−299.
(51) Khanipour, P.; Speck, F. D.; Mangoufis-Giasin, I.; Mayrhofer, K. J. J.; Cherevko, S.; Katsounaros, I. Electrochemical oxidation of isopropanol on platinum-ruthenium nanoparticles studied with real-time product and dissolution analytics. *ACS Appl. Mater. Interfaces* **2020**, *12*, 33670.
(52) Waidhas, F.; Haschke, S.; Khanipour, P.; Fromm, L.; Görling, A.; Bachmann, J.; Katsounaros, I.; Mayrhofer, K. J. J.; Brummel, O.; Libuda, J. Secondary Alcohols as Rechargeable Electrofuels: Electrooxidation of Isopropyl Alcohol at Pt Electrodes. *ACS Catal.* **2020**, *10* (12), 6831−6842.
(53) sun, S.-G.; Lin, Y. In situ FTIR spectroscopic investigations of reaction mechanism of isopropanol oxidation on platinum single crystal electrodes. *Electrochim. Acta* **1996**, *41* (5), 693−700.
(54) Jovanovič, P.; Ruiz-Zepeda, F.; Šala, M.; Hodnik, N. Atomic Scale Insights into Electrochemical Dissolution of Janus Pt−$SnO_2$ Nanoparticles in the Presence of Ethanol in Acidic Media: An IL-STEM and EFC−ICP−MS Study. *J. Phys. Chem. C* **2018**, *122* (18), 10050−10058.
(55) Chen, Y. X.; Heinen, M.; Jusys, Z.; Behm, R. J. Kinetics and mechanism of the electrooxidation of formic acid–spectroelectrochemical studies in a flow cell. *Angew. Chem., Int. Ed.* **2006**, *45* (6), 981−5.
(56) Chen, Y.; Zhou, Y.; Tang, Y.; Lu, T. Electrocatalytic properties of carbon-supported Pt-Ru catalysts with the high alloying degree for formic acid electrooxidation. *J. Power Sources* **2010**, *195* (13), 4129−4134.
(57) Jiang, Z.; Jiang, Z.-j. Improvements of electrocatalytic activity of PtRu nanoparticles on multi-walled carbon nanotubes by a H2 plasma treatment in methanol and formic acid oxidation. *Electrochim. Acta* **2011**, *56* (24), 8662−8673.
(58) Fayette, M.; Nutariya, J.; Vasiljevic, N.; Dimitrov, N. A Study of Pt Dissolution during Formic Acid Oxidation. *ACS Catal.* **2013**, *3* (8), 1709−1718.
(59) Colombo, C.; Oates, C. J.; Monhemius, A. J.; Plant, J. A. Complexation of platinum, palladium and rhodium with inorganic ligands in the environment. *Geochem.: Explor., Environ., Anal.* **2008**, *8* (1), 91−101.
(60) Swihart, D. L.; Mason, W. R. Electronic spectra of octahedral platinum (IV) complexes. *Inorg. Chem.* **1970**, *9* (7), 1749−1757.
(61) Katsounaros, I.; Figueiredo, M. C.; Calle-Vallejo, F.; Li, H.; Gewirth, A. A.; Markovic, N. M.; Koper, M. T. M. On the mechanism of the electrochemical conversion of ammonia to dinitrogen on Pt(100) in alkaline environment. *J. Catal.* **2018**, *359*, 82−91.
(62) Ye, J.-Y.; Lin, J.-L.; Zhou, Z.-Y.; Hong, Y.-H.; Sheng, T.; Rauf, M.; Sun, S.-G. Ammonia electrooxidation on dendritic Pt nanostructures in alkaline solutions investigated by in-situ FTIR spectroscopy and online electrochemical mass spectroscopy. *J. Electroanal. Chem.* **2018**, *819*, 495−501.
(63) Dinh, H. N.; Ren, X.; Garzon, F. H.; Zelenay, P.; Gottesfeld, S. Electrocatalysis in direct methanol fuel cells: in-situ probing of PtRu anode catalyst surfaces. *J. Electroanal. Chem.* **2000**, *491* (1−2), 222−233.
(64) Liao, M.-S.; Cabrera, C. R.; Ishikawa, Y. A theoretical study of CO adsorption on Pt, Ru and Pt−M (M = Ru, Sn, Ge) clusters. *Surf. Sci.* **2000**, *445* (2−3), 267−282.
(65) Green, C. L.; Kucernak, A. Determination of the Platinum and Ruthenium Surface Areas in Platinum−Ruthenium Alloy Electrocatalysts by Underpotential Deposition of Copper. I. Unsupported Catalysts. *J. Phys. Chem. B* **2002**, *106* (5), 1036−1047.
(66) Ochal, P.; Gomez de la Fuente, J. L.; Tsypkin, M.; Seland, F.; Sunde, S.; Muthuswamy, N.; Rønning, M.; Chen, D.; Garcia, S.; Alayoglu, S.; Eichhorn, B. CO stripping as an electrochemical tool for characterization of Ru@Pt core-shell catalysts. *J. Electroanal. Chem.* **2011**, *655* (2), 140−146.
(67) Chen, D. J.; Tong, Y. J. Irrelevance of Carbon Monoxide Poisoning in the Methanol Oxidation Reaction on a PtRu Electrocatalyst. *Angew. Chem., Int. Ed.* **2015**, *54* (32), 9394−8.
(68) Hofstead-Duffy, A. M.; Chen, D.-J.; Sun, S.-G.; Tong, Y. J. Origin of the current peak of negative scan in the cyclic voltammetry of methanol electro-oxidation on Pt-based electrocatalysts: a revisit to the current ratio criterion. *J. Mater. Chem.* **2012**, *22* (11), 5205.
(69) Joo, J.; Uchida, T.; Cuesta, A.; Koper, M. T. M.; Osawa, M. The effect of pH on the electrocatalytic oxidation of formic acid/formate on platinum: A mechanistic study by surface-enhanced infrared spectroscopy coupled with cyclic voltammetry. *Electrochim. Acta* **2014**, *129*, 127−136.
(70) Miki, A.; Ye, S.; Osawa, M. Surface-enhanced IR absorption on platinum nanoparticles: an application to real-time monitoring of electrocatalytic reactions. *Chem. Commun.* **2002**, *14*, 1500−1.
(71) Spendelow, J. S.; Lu, G. Q.; Kenis, P. J. A.; Wieckowski, A. Electrooxidation of adsorbed CO on Pt(111) and Pt(111)/Ru in alkaline media and comparison with results from acidic media. *J. Electroanal. Chem.* **2004**, *568*, 215−224.
(72) Kodama, K.; Morimoto, Y.; Strmcnik, D. S.; Markovic, N. M. The role of non-covalent interactions on CO bulk oxidation on Pt single crystal electrodes in alkaline electrolytes. *Electrochim. Acta* **2015**, *152*, 38−43.
(73) Schmidt, T. J.; Ross, P. N.; Markovic, N. M. Temperature-Dependent Surface Electrochemistry on Pt Single Crystals in Alkaline


https://dx.doi.org/10.1021/acscatal.0c02094
*ACS Catal.* 2020, 10, 10858−10870

Electrolyte: Part 1: CO Oxidation. *J. Phys. Chem. B* **2001**, *105* (48), 12082−12086.
(74) Corpuz, A. R.; Olson, T. S.; Joghee, P.; Pylypenko, S.; Dameron, A. A.; Dinh, H. N.; O'Neill, K. J.; Hurst, K. E.; Bender, G.; Gennett, T.; Pivovar, B. S.; Richards, R. M.; O'Hayre, R. P. Effect of a nitrogen-doped PtRu/carbon anode catalyst on the durability of a direct methanol fuel cell. *J. Power Sources* **2012**, *217*, 142−151.
(75) Kang, S.; Lim, S.; Peck, D.-H.; Kim, S.-K.; Jung, D.-H.; Hong, S.-H.; Jung, H.-G.; Shul, Y. Stability and durability of PtRu catalysts supported on carbon nanofibers for direct methanol fuel cells. *Int. J. Hydrogen Energy* **2012**, *37* (5), 4685−4693.


https://dx.doi.org/10.1021/acscatal.0c02094
*ACS Catal.* 2020, 10, 10858−10870